*The 2020 World Congress on*
***Advances in Civil, Environmental, & Materials Research (ACEM20)***
*25-28, August, 2020, GECE, Seoul, Korea*

# VIVs-Mechanism of a Streamlined Closed-box Girder Using a Simplified Vortex Model

*Chuanxin Hu[1)] and Lin Zhao[2)]

[1)] *Department of Civil Engineering, Wuhan University of Science and Technology, Wuhan 430065, China*
[2)] *State Key Lab of Disaster Reduction in Civil Engineering, Tongji University, Shanghai 200092, China*
[1)] *chuanxin86@126.com*

## ABSTRACT

The mechanism of vortex-induced vibrations (VIVs) in VIVs-development process and VIVs-suppression using aerodynamic countermeasures are critical for long-span bridges. Vortex-induced forces (VEFs), vortex-drifting pattern over the model surface, and model motion are close correlated, which are not clearly revealed and, may be helpful for understanding VIVs. A simplified vortex model, greatly simplifying the complex fluid-structure interactions between the model and surrounding flow, can be established by the vortexes over the model surface in a vibration period, from an energy perspective. Furthermore, aerodynamic parameters for the model are obtained from the spatial distribution of phase lags between the distributed aerodynamic forces at each tap and the general VEFs with help of spring-suspended sectional model (SSSM) wind tunnel tests of a streamlined closed-box girder. The results show that ratio of the vortex-drifting velocity to oncoming flow velocity, referred to as Strouhal number for the separated vortex, physically denotes energy characteristics of the work done by the vortex. Moreover, regular vortex-drifting pattern are dominant in vertical VIVs phenomena. However, VIVs at descent stage cannot be attributed solely to drift of large vortex along the body surface but rather some components irrelated to the vortex-drifting pattern. Spoilers on the handrails destroy obvious vortex-drifting pattern along the body surface, so vertical VIVs disappear.

## 1. INTRODUCTION

---

[1)] Ph. D
[2)] Professor

As the bridge span increases, the cable-supported bridge is widely used as a common structure, which is more flexible and has little damping capability. Therefore, dramatic wind-induced vibrations often occur on long-span cable-supported bridges. Among these vibrations, the frequent vortex-induced vibrations (VIVs) have attracted increasing attentions. The vertical VIVs have been found in many bridges including the Kessock Bridge in Scotland (Owen et al. 1996), the Storebælt Bridge in Denmark (Larsen et al. 2000; Frandsen 2014), the Rio-Niterói Bridge in Brazil (Battista and Pfeil 2000), the Trans-Tokyo Bay Highway Crossing in Japan (Fujino and Yoshida 2002), and the Xihoumen Bridge in China (Li et al. 2011; Li et al. 2014). On April 26th, 2020, vertical VIVs phenomena were observed in the Yingwuzhou Bridge, Hubei province, in China. Later, in Guangdong province, vertical VIVs phenomena were also observed in the Humen Bridge on June 5th. Although VIV is a kind of limited amplitude vibration and rarely causes collapse, it can result in large displacements and cause discomfort to drivers under lower wind velocity conditions, and reduce fatigue life to some extent.

There are two different vortex excitations for elongated sharp-edged bluff girders (e.g., typical bridge decks), i.e. the one-shear-layer vortex-related excitation and the Karman vortex-related excitation (Matsumoto 1999). Both were believed to be the triggering mechanism for VIVs phenomena (Nakamura and Nakashima 1986). Bridge girders with the characteristics of large aspect ratio are more prone to the former excitation. Rockwell and Naudascher 1978 found that the separated shear layer issuing from the upstream corner of a cavity often becomes unstable to roll-up in discrete vortices in the presence of the downstream corner. Such a flow instability, which belongs to a more general class of flow instabilities related to jets and wakes, is herein referred to as the impinging-shear-layer instability. Kubo et al. 1992 reported on flow-visualization experiments with H-shaped sections. They demonstrated experimentally the existence of the large vortices and identified a link between the mode of aerodynamic excitation (torsional or vertical motion) and the vortex pattern forming along the girders. They also proposed that the vortices observed travel along the cross section with a constant velocity proportional to the velocity of the onset flow. Furthermore, Larsen 2000 firmly link the formation of vortex-drifting pattern to the time-dependent aerodynamic forces acting on the girder and, through a simple model, and then to link the vortex-drifting pattern to onset wind velocity of flutter instability. Hu and Zhao et al. 2019 associated vortex-drifting pattern, called “double vortex model” by them, with the time-frequency characteristics of aerodynamic forces around a streamlined closed-box girder, to reveal VIV suppression mechanism of aerodynamic measurements for that bridge girder. In conclusion, Vortex-induced forces, vortex-drifting pattern, and model motion are close correlated, which are not clearly reveal and, may be helpful for understanding VIVs. However, they have not closely correlated the vortex-drifting pattern with VIVs in VIV-development process and VIVs-suppression to some extent, especially “lock-in” phenomena of VIVs.

The aim of this paper is to reveal the vertical VIVs in VIVs-development process and VIVs-suppression mechanism of a bridge girder with a streamlined closed-box cross-section with help of wind tunnel tests of the spring-suspended sectional model (SSSM), in terms of relationships between vortex-drifting pattern and model motion, which is also close correlated with the time-frequency characteristics of general and distributed aerodynamic forces around the section, called simplified vortex model here.

## 2. SIMPLIFIED VORTEX MODEL

In this section, an H-shaped section is taken as example to illustrate the simplified vortex model, greatly simplifying the complex fluid-structure interactions between the model and surrounding flow, and can be described by the vortexes over the model surface in a vibration period (Larsen 2000), as shown in Figure 1. It should be noted that the vortexes in Figure 1 are simplified vortexes, which is somewhat different from those in the flow field. In addition to the assumptions made by Larsen 2000, we also assume that the force vortexes acting on the model surface are independent of the path, which are called conservative force.

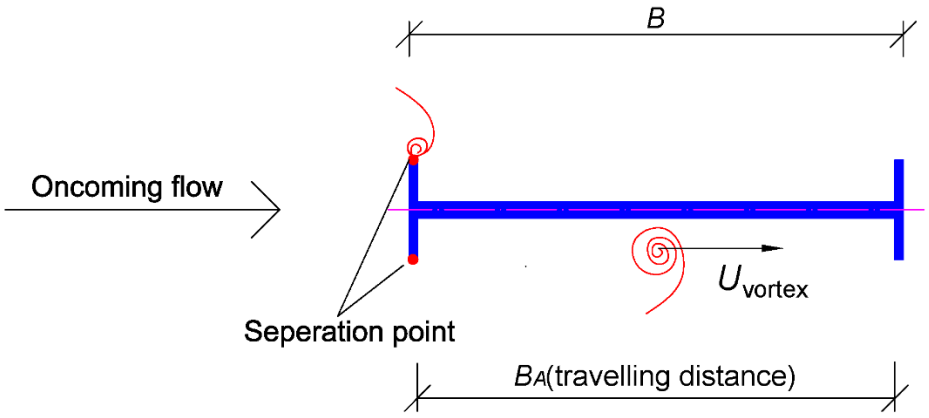


Figure 1: Schematic of the simplified vortex model

According to Shiraishi and Matsumoto 1983, a leading edge vortex with travelling velocity ($U_{vortex}$), reaches the trailing edge after $n$ cycle of the vertical motion to coalesce with the trailing edge vortex. Vortex-drifting pattern and associate work in a vertical vibration circle in $W_\alpha$=0 and $n$=1 situation are illustrated in Figure 2 and Figure 3 respectively, ignoring roles of trailing edge vortex. It is obviously that the work vortexes do to the model in a vibration period is zero.

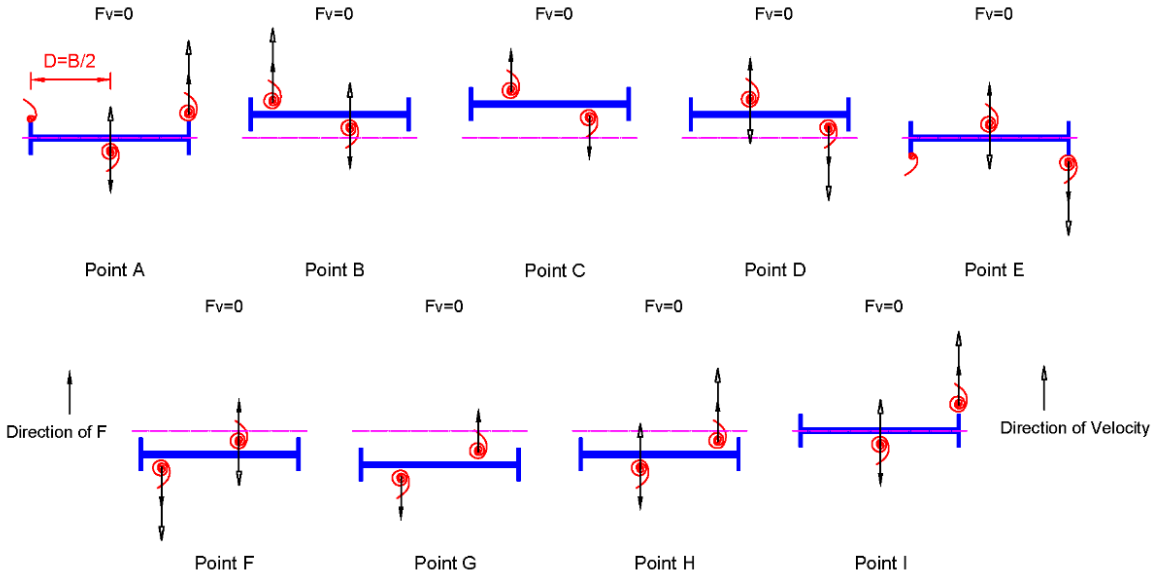


Figure 2: Vortex-drifting pattern ($W_\alpha$=0 and $n$=1) in the case of onset of vertical VIVs

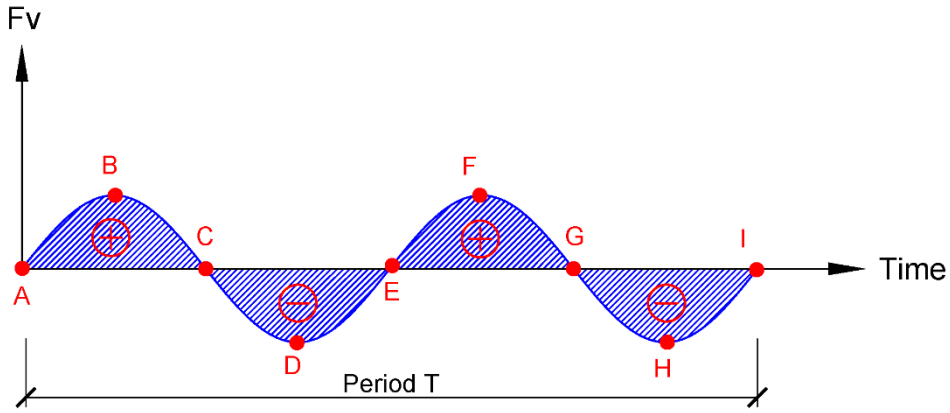


Figure 3: Work in a circle of vertical vibration ($W_\alpha$=0)

As shown in Figure 2, the relationships between travelling velocity ($U_{\text{vortex}}$) and vibration frequency can be described as follows:

$$nU_{\text{vortex}}T_{\text{v}}=B_{\text{A}} \tag{1}$$

Where $n=1, 2, 3, ....$, $B_{\text{A}}$ is the travelling distance of the vortex, $T_{\text{v}}$ is the vibration period. Then onset reduced velocity for the vertical VIVs ($U_{\text{cr}}^{*}$) can be expressed as:

$$U_{\text{cr}}^{*}=\frac{U}{f_{\text{v}}B}=\frac{U}{nU_{\text{vortex}}}\frac{B_{\text{A}}}{B} \tag{2}$$

Where $B$ is the model width. And Strouhal number for the separated vortex in this case could be defined as:

$$St^{*}=\frac{nU_{\text{vortex}}}{U} \tag{3}$$

Then onset reduced velocity for the vertical VIVs can be rephrased as:

$$U_{\mathrm{cr}}^{*}=\frac{1}{St^{*}}\frac{B_{\mathrm{A}}}{B} \tag{4}$$

For the bridge girder like H-shaped section, travelling distance of the vortex ($B_{\mathrm{A}}$) approximately equals to model width ($B$). Therefore, Eq. (4) can be rewritten as follows:

$$U_{\mathrm{cr}}^{*}=\frac{1}{St^{*}} \tag{5}$$

Eq. (5) is equivalent to that proposed by Shiraishi and Matsumoto 1983 to get onset reduced velocity of VIVs in vertical direction. Note that the separated vortex is related to the enhancement of the shear layer instability and then motion-induced, so they are obviously different from the well-known Karman vortex shedding (KV). Moreover, there are two types of Strouhal number, one for separated vortexes, one for Karman vortex, both can lead to vortex-induced vibrations (Matsumoto et al. 1993). Obviously, these characteristics clearly show that two different vortex excitations exist, i.e. the one-shear-layer vortex-related response and the Karman vortex excitation. Both can be characterized by equation (4), i.e., the reciprocal of the Strouhal number.

As for an H-shaped section with an aspect ratio in the range of 2 to 7.5, ratio of the vortex-drifting velocity along the model surface to oncoming wind velocity is nearly a constant, and takes value of approximately 0.6 (Shiraishi and Matsumoto 1983; Matsumoto 1999; Matsumoto et al. 1993). Therefore, onset reduced velocity of vertical VIVs can be rewritten as:

$$U_{\mathrm{cr}}^{*}=\frac{1}{0.6n}\quad(n=1,2,3\ldots) \tag{6}$$

When $n$ takes the value of 1 and 2, onset reduced velocity of vertical VIVs $U_{\mathrm{cr}}^{*}$ is 1.7 and 0.8, consistent with the experimental results (Shiraishi and Matsumoto 1983; Matsumoto 1999; Matsumoto et al. 1993).

Hu and Zhao 2018, 2019 proposed “contribution values” to reveal evolutionary characteristics of aerodynamic forces in the VIV-development process, VIV-triggering and VIV-suppression mechanism, combined with phase lags between the distributed aerodynamic forces and the general VEFs ($\varphi_{DtoG}$). However, the relationships between the contribution values and work done to the model has not been clarified, which is critical for understanding nonlinear characteristics of aerodynamic forces. The relationships among these phase lags can be expressed as follows:

$$\varphi_{DtoM}+\varphi_{MtoG}=\varphi_{DtoG} \tag{7}$$

Where, $\varphi_{DtoM}$ denotes phase lags between local distributed aerodynamic forces and model motion; $\varphi_{DtoG}$ denotes phase lags between the distributed aerodynamic forces and the general VEFs; $\varphi_{MtoG}$ denotes phase lags between model motion and the general VEFs. If only $\varphi_{MtoG}$ equals to 0, $\varphi_{DtoM}$ equals to $\varphi_{DtoG}$. Then work distribution are equivalent to contribution coefficients distribution. It is natural that the spatial distribution of contribution values differs from that of work. Moreover, overall offset of phase lags between local aerodynamic forces and the general VEFs actually means overall offset of phase lags between local aerodynamic forces and the model motion, indicating that variation of contribution values can reflect variation of work to some extent.

Furthermore, variations of phase lags between local distributed aerodynamic forces and model motion or phase lags between the distributed aerodynamic forces and the general VEFs along the model surface actually represent vortex-drifting, as shown in Figure 4. Then, the time it takes for the vortex to drift from point A to point B can be expressed as:

$$\Delta t = \frac{\Delta\varphi}{360} T_{\mathrm{V}} \tag{8}$$

$$\Delta\varphi = \varphi_{\mathrm{B}} - \varphi_{\mathrm{A}} \tag{9}$$

Where, $\varphi_{\mathrm{B}}$ and $\varphi_{\mathrm{A}}$ denotes phase lag (phase lag between local distributed aerodynamic forces and model motion or phase lag between the distributed aerodynamic forces and the general VEFs) at point B and point A, respectively. Then, travelling velocity ($U_{\mathrm{vortex}}$) can be get as follows:

$$U_{\mathrm{vortex}} = \frac{\Delta D}{\Delta t} \tag{10}$$

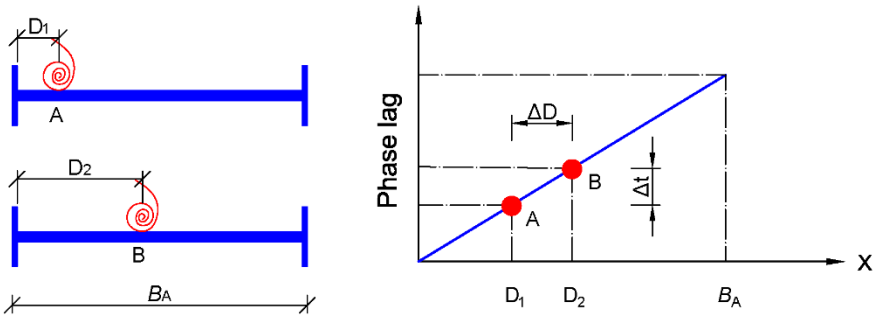


Figure 4: Variation of travelling distance with phase lag

## 3. VIV-TRIGGERING MECHANISM

A traditional streamlined closed-box girder of long-span bridges with a width (B) of 38.0 m and a depth (D) of 3.1 m here is taken as research object. The aspect ratio of the bridge girder is roughly 7.5:1, accounting for attachments, as shown in Figure 5 and Figure 6. Wind tunnel tests of synchronal measurement of pressures and displacement responses of spring-suspended sectional model with scales of 1:20 and 1:70 were conducted, with Reynolds number of $6.08\times10^{3}$~$2.28\times10^{4}$ and $1.06\times10^{4}$~$1.40\times10^{5}$ respectively. All details concerning the experimental arrangement are described in Hu and Zhao 2018, 2019.

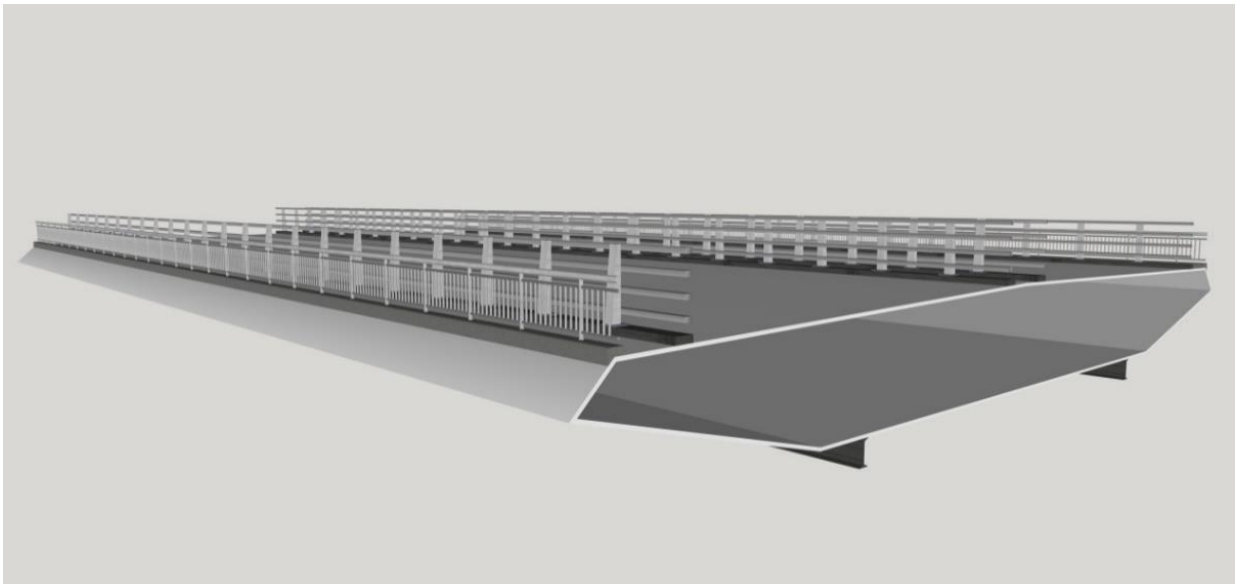

Figure 5: Layouts of attachments on bridge girder

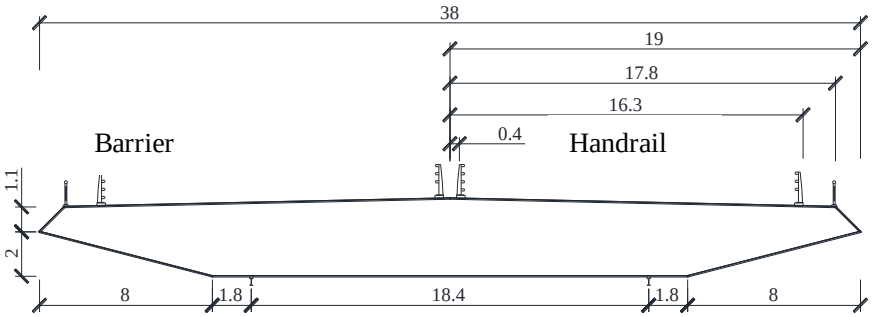


(a) Overall

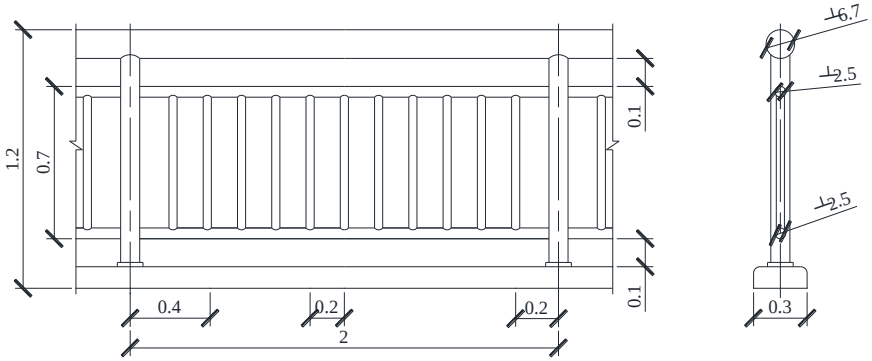


(b) Handrail

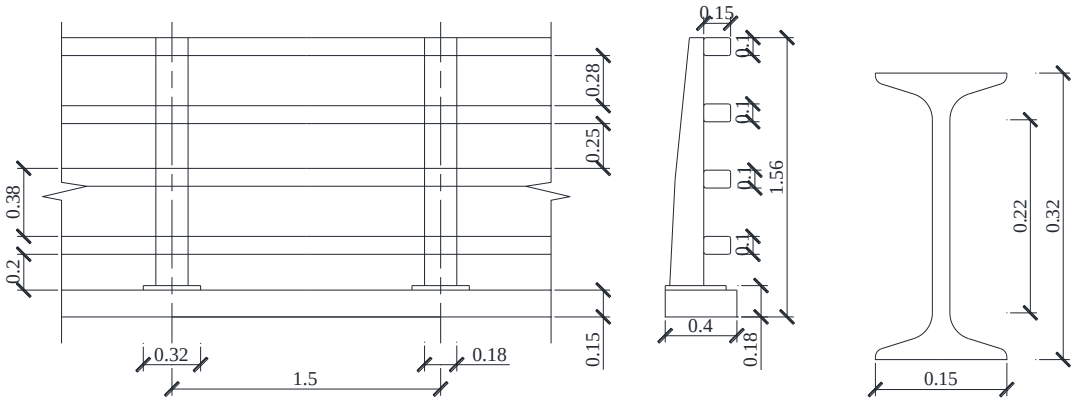


(c) Barrier (d) Maintenance trace

Figure 6: Geometrical sizes of a bridge deck (Unit: m)

The VIV responses at an attack angle of + 3° are shown in Figure 7, in which $U_{\mathrm{A}}^{*}=U/\left(f_{\mathrm{h}}B_{\mathrm{A}}\right)$ denotes actual reduced velocity, $B_{\mathrm{A}}$ denotes travelling distance of the vortex, as shown in Figure 8. $A$ is the amplitude of vertical VIV response, and $A/D$ is normalized amplitude. There are two vertical lock-in regions in the range of actual reduced velocity, and corresponding onset actual critical reduced velocity is 0.91, 1.71, respectively. The first is in the range of 0.91~1.13, while the 2nd ranges from 1.71 to 2.36, with a maximal normalized amplitude of 0.067 at a reduced velocity of 2.26.

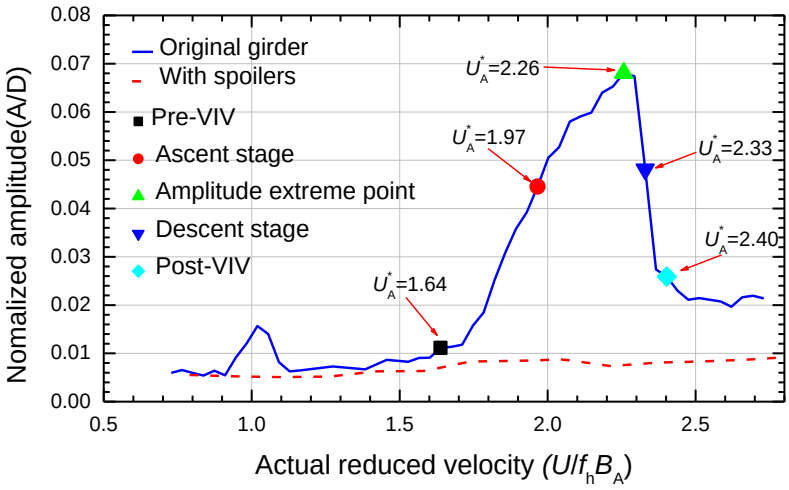


Figure 7: Vertical amplitudes of model displacements in VIV-development process

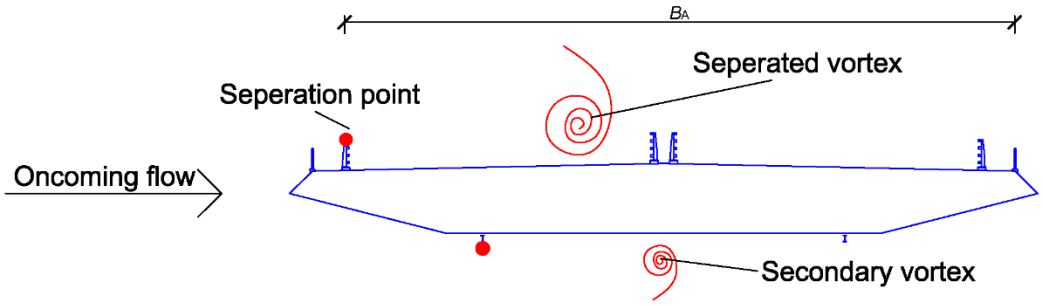


Figure 8: Schematic of the simplified vortex model for the streamlined closed box girder

Power spectra density of the VEFs on the model surface at a reduced velocity of 1.64 when the model is at stationary state is shown in Figure 9. There are obviously peaks at frequency of 1.684Hz, 5.469Hz and 10.083Hz, and corresponding actual Strouhal numbers are 0.181, 0.589, and 1.09, respectively. Thus, the actual onset wind velocity of VIVs could be calculated as 5.52, 1.70, 0.92 respectively, providing that vortices relating to Strouhal numbers above are sufficiently enough to excite the oscillations, according to Eq. (5). The calculated actual onset reduced velocities above for the last two Strouhal numbers approximately agree with the measured actual onset reduced velocities of VIVs in Figure 9, indicating that the first and second lock-in regions are triggered by the different vortices with different Strouhal numbers.

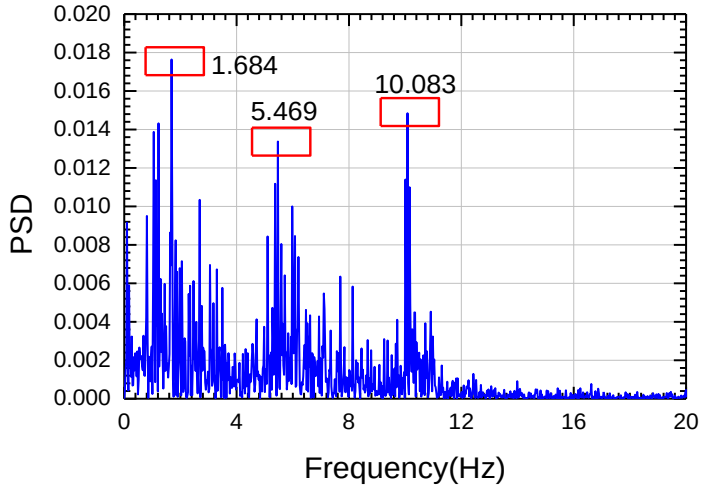


Figure 9: Power spectra density functions of the VEFs on the model surface at an actual reduced velocity of 1.64 ($U_{\mathrm{A}}^{*}$=1.64) when model is at stationary state

Spoilers of 30° inclination are installed on top of the handrails to suppress the vertical VIVs for the original cross section, as shown in Figure 10, and displacements are illustrated in Figure 9. The VIV phenomena, including the first and second lock-in regions, disappeared when spoilers were set, indicating that both lock-in regions are mainly triggered by the Kelvin-Helmholtz instability due to the single separating shear layer instability around the bridge deck, referred to as the impinging-shear-layer instability (Rockwell and Naudascher 1978; Nakamura and Nakashima 1986).

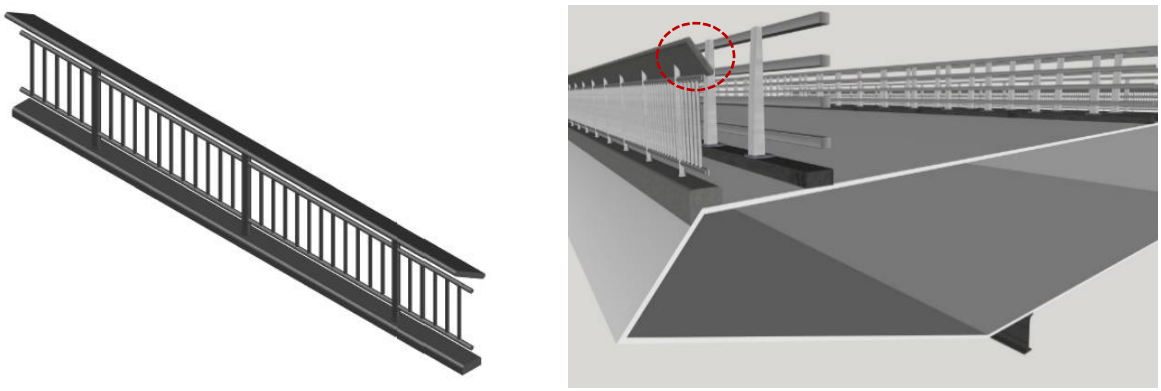

Figure 10: Modified cross section with spoilers of 30° inclination

Only part of VIV phenomena (in this case, only the 2nd lock-in region) is analyzed to reveal VIVs mechanism. Some case studies for reduced velocities of 1.64, 1.97, 2.26, 2.32 and 2.40, representing pre-VIV stage, ascent stage, amplitude extreme point, descent stage, and post-VIV stage, respectively are analyzed in this paper. According to equations in Section 2, aerodynamic parameters for the simplified vortex model in VIV-development process can be obtained, as shown in Table 1. Note that Strouhal number for the vortex ($St^*$) at pre-VIV stage is in well coincidence with the Strouhal number measured in Figure 9, further indicating that the vertical VIVs are mainly triggered by the Kelvin-Helmholtz instability due to the impinging-shear-layer instability. It is observed that drifting velocity of the vortex increases as actual reduced velocity. Moreover, calculated reduced velocities obtained from the simplified vortex model by Eq. (5) agree well with the actual reduced velocities in VIV-development process, indicating that regular vortex-drifting pattern are dominant in VIVs-development process. However, there are larger discrepancy between calculated reduced velocities and the actual reduced velocities at descent stage and post-VIV stage, compared with other stages. Therefore, VIVs at descent stage are not solely cannot be attributed solely to drift of large coherent vortex structures along the body surface but rather some components irrelated to the vortex-drifting pattern. In conclusion, vertical VIVs are mainly triggered and maintained by the regular vortex-drifting pattern in VIV-development. And VIVs at ascend stage and descend stage are slightly different in terms of vortex-drifting pattern, which may be responsible for lock-in phenomena of VIVs.

Table 1: Aerodynamic parameters of the simplified vortex model in VIV-development process

| VIV-development process | Actual reduced velocity ($U_A^*$) | Vortex-drifting velocity $U_{vortex}$ (m/s) | Strouhal number ($St^*$) | Calculated reduced velocity | Error (%) |
|---|---|---|---|---|---|
| Pre-VIV stage | 1.64 | 2.50 | 0.556 | 1.80 | 9.8 |
| Ascent stage | 1.97 | 2.71 | 0.502 | 1.99 | 1.0 |
| Amplitude extreme point | 2.26 | 2.91 | 0.470 | 2.13 | -5.8 |

| | | | | | |
|---|---|---|---|---|---|
| Descent stage | 2.33 | 3.13 | 0.490 | 2.04 | -12.4 |
| Post-VIV stage | 2.40 | 3.23 | 0.489 | 2.05 | -14.6 |

## 4. VIV-SURPPRESSION MECHANISM

Figure 10 shows the phase lags between the distributed aerodynamic forces at each pressure tap and the general VEFs at predominant frequency for the unmodified bridge girder and modified bridge girders. For the unmodified bridge girder, the phase lags between the aerodynamic forces and the general VEFs in the downstream region of surface ② vary linearly in the range of -90°~60°. Similarly, the phase lags on the model surface also appear as a linear continuous distribution after guide vanes are installed, and have an overall offset of about 90° with respect to the unmodified bridge girder. With spoilers, the phase lags of the bridge girder are different from those of the other bridge girders. Therefore, there are obviously vortex-drifting pattern over the upper surface of the model in the VIV-development process for the original girder and guide vane girder, which is responsible for vertical VIVs of these girders. However, there are no obvious vortex-drifting pattern due to spoilers on the handrails.

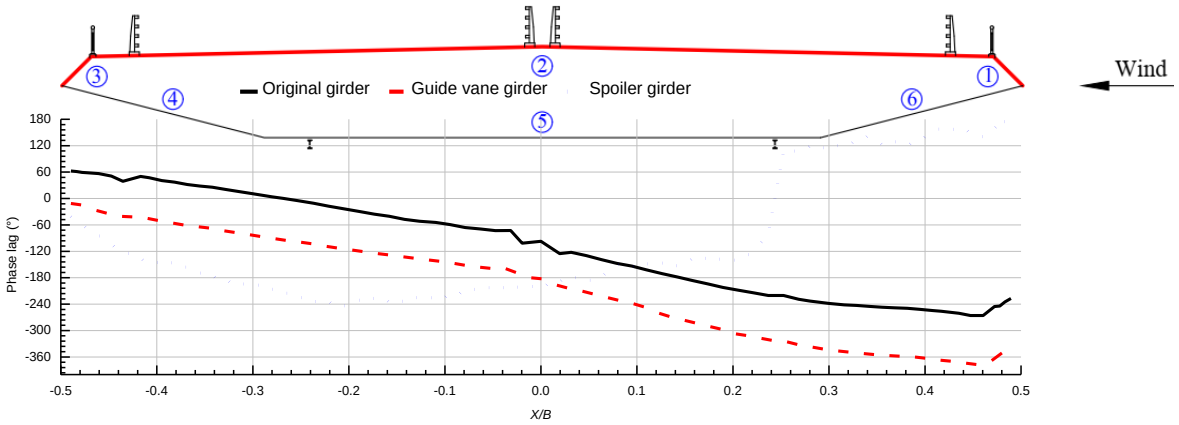


Figure 11: Phase lags between distributed aerodynamic forces at each pressure tap over the upper surface and general VEFs at predominant frequency

Furthermore, aerodynamic parameters for the simplified vortex model of the original girder and guide vane girder can be obtained according to equations in Section 2, and are listed in Table 2. Calculated reduced velocities obtained from the simplified vortex model by Eq. (5) show well coincidence with the actual reduced velocities. It is also observed that Strouhal number ($St^*$) for the original girder agree well with that for the Guide vane girder.

Table 2: Aerodynamic parameters of the simplified vortex model

| Bridge girder | Actual reduced velocity ($U_A^*$) | Vortex-drifting velocity $U_{vortex}$ (m/s) | Strouhal number ($St^*$) | Calculated reduced velocity | Error (%) |
|---|---|---|---|---|---|

| | | | | | |
|---|---|---|---|---|---|
| Original girder | 2.23 | 6.37 | 0.51 | 1.96 | -12.1 |
| Guide vane girder | 2.10 | 5.85 | 0.50 | 2.02 | -3.8 |

## 5. CONCLUSIONS

In order to reveal the mechanism of VIVs in VIV-development process and VIVs-suppression mechanism of a streamlined closed-box girder with the addition of some typical small-scale aerodynamic countermeasures involving spoilers on barriers and guide vanes near maintenance trails, time-frequency characteristics of aerodynamic forces around a bridge girder are used to were utilized to analyze vortex-drifting pattern around the bridge girder with help of a simplified vortex model. Some main conclusions are as follows:

1) A simplified vortex model, greatly simplifying the complex fluid-structure interactions between the model and surrounding flow, can be established by the vortex over the model surface in a vibration period, from an energy perspective. Ratio of the vortex-drifting velocity to oncoming flow velocity, referred to as Strouhal number for the separated vortex, physically denotes energy characteristics of the work done by the vortex.
2) Drifting velocity of the vortex in VIV-development increases as actual reduced velocity. Regular vortex-drifting pattern are dominant in vertical VIVs phenomena. However, VIVs at descent stage cannot be attributed solely to drift of large vortex along the body surface but rather some components irrelated to the vortex-drifting pattern.
3) Spoilers on the handrails destroy obvious vortex-drifting pattern along the body surface, so vertical VIVs disappear.

## REFERENCES

Owen, J. S., Vann, A. M., Davies, J. P., and Blakeborough, A. (1996), “The prototype testing of Kessock Bridge: Response to vortex shedding”, *J. Wind Eng. Ind. Aerodyn.*, **60**, 91–108.

Larsen, A., Esdahl, S., Andersen, J.E., Vejrum, T. (2000). “Storebælt suspension bridge vortex shedding excitation and mitigation by guide vanes”, *J. Wind Eng. Ind. Aerodyn.*, **88**(2), 283–296.

Frandsen, J. B. (2014), “Simultaneous pressures and accelerations measured full-scale on the Great Belt East suspension bridge”, *J. Wind Eng. Ind. Aerodyn.*, **89**(1), 95–129.

Battista, R.C., Pfeil, M.S. (2000), “Reduction of vortex-induced oscillations of Rio–Niterói bridge by dynamic control devices”, *J. Wind Eng. Ind. Aerodyn.*, **84**(3), 273-288.

Fujino, Y., Yoshida, Y. (2002), “Wind-induced vibration and control of trans-Tokyo Bay crossing bridge”, Journal of Structural Engineering, **128**(8), 1012-1025.

Li, H., Laima, S., Ou, J., Zhao, X., Zhou, W., Yu, Y., et al. (2011), “Investigation of vortex-induced vibration of a suspension bridge with two separated steel box girders based on field measurements”, Engineering Structures, **33**(6), 1894-1907.

Li, H., Laima, S. J., and Zhang, Q. Q. (2014), "Field monitoring and validation of vortex-induced vibrations of a long-span suspension bridge", *J. Wind Eng. Ind. Aerodyn.*, **124**, 54–67.

Matsumoto, M. (1999), "Vortex shedding of bluff bodies: a review", Journal of Fluids & Structures, **13**(7-8), 791-811.

Nakamura Y., Nakashima M., 1986. "Vortex excitation of prisms with elongated rectangular, H and h cross-sections", Journal of Fluid Mechanics, **163**, 149–169.

Rockwell, D., Naudascher, E., 1978. "Review - self-sustaining oscillations of flow past cavities", Asme Transactions Journal of Fluids Engineering, 100(2), 152-165.

Kubo, Y., Hirata, K., and Mikawa, K. (1992), "Mechanism of aerodynamic vibrations of shallow bridge girder sections", J. Ind. Aerodyn., **42**(1), 1297-1308.

Larsen, A. (2000), "Aerodynamics of the Tacoma Narrows Bridge - 60 years later", Structural Engineering International, **10**(4), -.

Hu, C.X., Zhao, L., and Ge, Y.J. (2018), "Time-frequency evolutionary characteristics of aerodynamic forces around a streamlined closed-box girder during vortex-induced vibration", *J. Wind Eng. Ind. Aerodyn.*, **182**, 330-343.

Hu, C.X., Zhao, L., and Ge, Y.J. (2019), "Mechanism of Suppression of Vortex-induced Vibrations of a Streamlined Closed-box Girder using Additional Small-scale Countermeasures", *J. Wind Eng. Ind. Aerodyn.*, **189**, 314-331.

Shiraishi N., and Matsumoto M. (1983), "On classification of vortex-induced oscillation and its application for bridge structures", *J. Wind Eng. Ind. Aerodyn.*, **14**(1), 419-430.

Matsumoto M. (1999), "Vortex shedding of bluff bodies: A review", Journal of Fluids and Structures, **13**(7-8), 791-811.

Matsumoto, M., Shiraishi, N., Shirato, H., Stoyanoff, S., and Yagi, T. (1993), "Mechanism of, and turbulence effect on vortex-induced vibrations for bridge box girders", J. Ind. Aerodyn., **49**(1-3), 467-476.